The winter Arctic Oscillation, the timing of spring, and carbon fluxes in the Northern Hemisphere

Kevin Schaefer, A. Scott Denning, and Owen Leonard

Department of Atmospheric Science, Colorado State University, Fort Collins, Colorado, USA

Received 9 July 2004; revised 4 April 2005; accepted 14 June 2005; published 27 August 2005.

[1] Various observations show trends toward warmer and earlier springs in the Northern Hemisphere. We hypothesize that the positive trend in the winter Arctic Oscillation (AO) has led to higher winter temperatures, advanced spring, and increased seasonal amplitudes in atmospheric CO_2. To test this hypothesis, we modeled leaf-out and terrestrial carbon fluxes using the Simple Biosphere model, Version 2 (SiB2) and the National Centers for Environmental Prediction (NCEP) reanalysis for 1958–2002. We found that our modeled leaf-out trends were consistent with observed phenology and that the winter AO trend can statistically explain 20–70% of the modeled leaf-out trends in the eastern United States and northern Europe. We also found that warmer winter temperatures associated with the positive trend in the winter AO increased winter respiration. At the same time, these warmer winter temperatures advanced the date of leaf-out, increasing the total spring uptake of atmospheric CO_2 by plants. These seasonally asymmetric trends toward increased respiration in winter and increased photosynthesis in spring can help explain the trend toward increased seasonal amplitudes in observed atmospheric CO_2 concentration.

Citation: Schaefer, K., A. S. Denning, and O. Leonard (2005), The winter Arctic Oscillation, the timing of spring, and carbon fluxes in the Northern Hemisphere, *Global Biogeochem. Cycles*, *19*, GB3017, doi:10.1029/2004GB002336.

1. Introduction

[2] Over the last half of the twentieth century, trends in various observations indicate warmer winters and earlier springs in the Northern Hemisphere [*Serreze et al.*, 2000]. The seasonal amplitude of atmospheric CO_2 concentration has increased and the phasing has advanced earlier in spring [*Keeling et al.*, 1995, 1996]. Flowering, leaf-out, and other spring phenophases (climate driven growth or senescence events) have advanced, indicating a longer growing season [*Menzel and Fabian*, 1999; *Keyser et al.*, 2000; *Menzel*, 2000, 2003]. Satellite derived Normalized Difference Vegetation Index (NDVI) has increased, indicating greener plants, earlier springs, and longer growing seasons [*Myneni et al.*, 1997; *Slayback et al.*, 2003]. The wintertime Arctic Oscillation (AO), the dominant mode of variability in the Northern Hemisphere, has tended toward positive polarity since the 1960s [*Thompson et al.*, 2000]. We hypothesize that trends toward earlier springs, increased amplitudes in atmospheric CO_2, and higher NDVI are related to the trend in the winter AO.

[3] Since the 1960s, the atmospheric CO_2 seasonal amplitude has increased 20% in Hawaii and 40% in the arctic. The phasing of the CO_2 seasonal cycle has also advanced 7 days globally, indicating an earlier spring [*Keeling et al.*, 1995, 1996; *Randerson et al.*, 1999]. On the basis of monthly averages of observed concentration obtained from flask samples from National Oceanic and Atmospheric Administration (NOAA) Climate Monitoring and Diagnostics Laboratory (CMDL) Carbon Cycle Cooperative Global Air Sampling Network [*Conway et al.*, 1994], the average CO_2 seasonal amplitude is about 15 ppm at Barrow Alaska, and 6 ppm at Mauna Loa, Hawaii (Figure 1). The seasonal variability in observed carbon dioxide concentrations from flasks is driven by plant growth in the Northern Hemisphere. CO_2 decreases in spring and early summer as photosynthesis in the Northern Hemisphere terrestrial biosphere draws CO_2 out of the atmosphere. CO_2 increases the rest of the year when respiration puts CO_2 back into the atmosphere [*Keeling et al.*, 1996; *Wu and Lynch*, 2000]. Recent studies indicate that the trend toward increased drawdown in spring has slowed or even stopped [*Angert et al.*, 2004; *Russell and Wallace*, 2004]. Nevertheless, most high latitude sites show positive trends in the seasonal CO_2 amplitude (annual maximum minus minimum CO_2 concentration), although only the trend at Barrow, Alaska is statistically significant (Figure 2).

[4] CO_2 amplitude trends might result from seasonally asymmetric trends in the net terrestrial CO_2 fluxes [*Zimov et al.*, 1996; *Wu and Lynch*, 2000]. Seasonally asymmetric trends are tendencies that are stronger or even of opposite sign at different times of the year. Correlations between temperature and regional net carbon flux (obtained by inverting flask measurements with a transport model) indicate enhanced late spring and early summer photosynthesis

0886-6236/05/2004GB002336$12.00

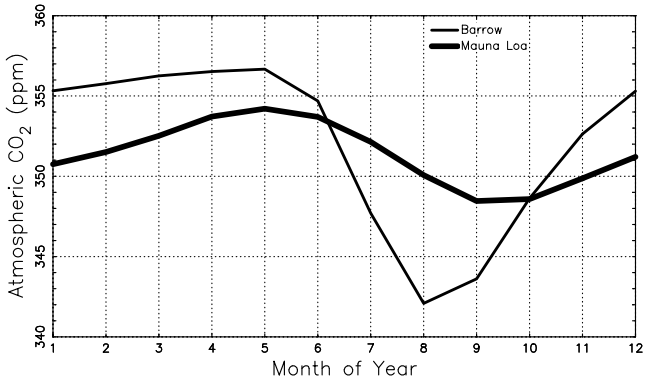

Figure 1. Average, annual seasonal cycles in observed atmospheric CO_2 concentration (ppm) at Barrow, Alaska, and Mauna Loa, Hawaii.

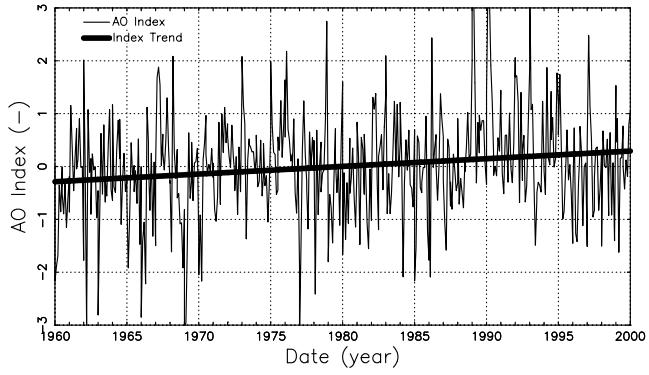

Figure 3. Monthly average Arctic Oscillation (AO) index and associated trend based on the first principle component of sea level pressure from the NCEP reanalysis.

best reproduces the observed trend in CO_2 amplitude [*Randerson et al.*, 1999]. Trends toward increased GPP in spring would amplify the drawdown, resulting in a lower minimum CO_2. Likewise, trends toward increased respiration at other times of the year would amplify the CO_2 buildup, resulting in a higher maximum CO_2. Alternatively, changes in the timing of peak photosynthesis and respiration rates could also change the CO_2 amplitude even though the annual net annual carbon exchange may not change [*Idso et al.*, 1999; *Wu and Lynch*, 2000; *Lucht et al.*, 2002; *Nemani et al.*, 2002]. For example, advanced snowmelt in spring could advance peak photosynthesis in early summer [*Chapin et al.*, 1996; *Stone et al.*, 2002]. Lastly, changes in seasonal patterns of atmospheric circulation may shift the source regions observed by flask stations, resulting in a trend in the observed CO_2 amplitude [*Dargaville et al.*, 2000; *Higuchi et al.*, 2002].

[5] Warmer temperatures in early spring have advanced observed leaf-out and other spring phenophases in Europe and North America since the 1950s. Trends in autumn phenophases are not as clear, with some species advancing and others retreating, but overall show delays of 4.8 days in Europe. From 1959 to 1996 in Europe, the average growing season has increased by 10.8 days. Since early spring phenophases show the strongest trends, the longer growing seasons are due primarily to earlier starts in spring [*Menzel and Fabian*, 1999; *Keyser et al.*, 2000; *Menzel*, 2000; *Schwartz and Reiter*, 2000; *Menzel*, 2003].

[6] NDVI data sets for 1982–2000 with various corrections all show statistically significant positive trends in the Northern Hemisphere, indicating earlier greening, later falls, and lengthening growing seasons [*Myneni et al.*, 1997; *Los et al.*, 2001; *Tucker et al.*, 2001; *Zhou et al.*, 2001; *Hicke et al.*, 2002a, 2002b; *Shabanov et al.*, 2002; *Slayback et al.*, 2003; *Zhou et al.*, 2003]. The exception is one NDVI data set that did not correct for sensor drift and calibration [*Slayback et al.*, 2003]. The NDVI trends persist all year, although the greatest increases occur in Eurasian boreal zones in March, April, and May. Warming in spring and fall statistically explain the largest fraction of the greening trend [*Tucker et al.*, 2001; *Nemani et al.*, 2002; *Zhou et al.*, 2001; *Slayback et al.*, 2003; *Zhou et al.*, 2003].

[7] Interpretation of the NDVI trends is difficult. On the basis of individual band reflectances and a radiative transfer model, the increased NDVI in spring can be explained by darker soils from decreased snow cover [*Shabanov et al.*, 2002], which would mask relationships between NDVI and plant phenophases [*Chen and Pan*, 2002]. Also, the monthly or bi-monthly NDVI time resolution is too coarse to detect trends in plant phenophases and the record too short to form strong conclusions [*White et al.*, 1997; *Serreze et al.*, 2000; *Zhou et al.*, 2001; *Chen and Pan*, 2002]. Nevertheless, the NDVI trends are consistent with increasing photosynthetic activity in spring and summer and with the observed increase in the CO_2 seasonal amplitude [*Ichii et al.*, 2001; *Shabanov et al.*, 2002; *Slayback et al.*, 2003].

[8] The AO, the dominant atmospheric circulation mode in the Northern Hemisphere, is a zonally symmetric "seesaw" in atmospheric mass between the Arctic and midlatitudes. Positive AO polarity has lower pressure in the Arctic and higher pressure at 45°N. Geostrophic balance dictates that positive AO polarity produces smoother zonal flow with stronger westerly winds north of 45°N and weaker

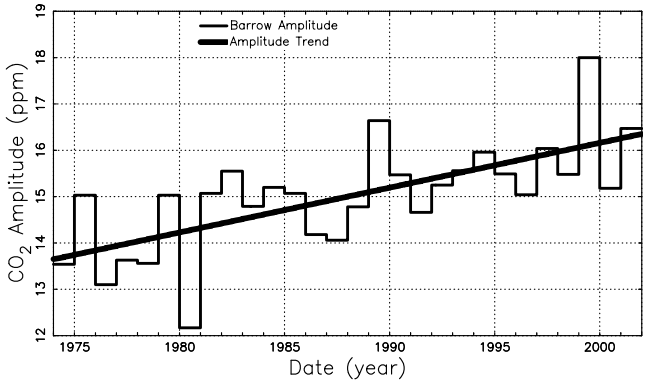

Figure 2. Amplitudes of annual seasonal cycles of observed atmospheric CO_2 concentration (ppm) and associated trend at Barrow, Alaska. Amplitude is annual maximum minus minimum CO_2 concentration. The trend is statistically significant.

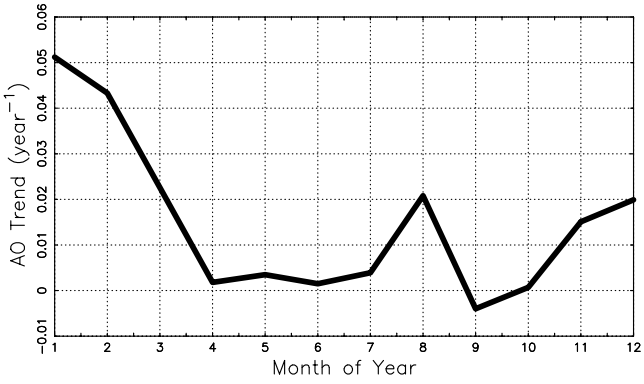

Figure 4. Monthly trends in the AO index (yr^{-1}). Only January, February, and August trends are statistically significant.

westerly winds south of 45°N. The AO randomly switches polarity with a characteristic synoptic timescale of 7–10 days. The AO exists year-round, but is strongest and most variable in winter, when radiative cooling over the pole is greatest and the polar vortex is strongest. The AO weakens in March as the polar vortex breaks down [*Thompson et al.*, 2000; *Thompson and Wallace*, 2000, 2001].

[9] Since late 1960s, the wintertime AO has exhibited a trend toward positive polarity [*Thompson et al.*, 2000], indicating a gradual strengthening of the wintertime polar vortex [*Serreze et al.*, 2000]. Figure 3 shows a monthly average AO index based on the first principle component of sea level pressure from the National Centers for Environmental Prediction (NCEP) reanalysis [*Thompson and Wallace*, 2000]. The monthly AO index is very noisy, as expected for a synoptic timescale phenomenon, but does show an overall trend toward positive polarity. The overall linear trend in Figure 3 is dominated by strong, statistically significant trends in January and February, although August also shows a positive, statistically significant trend (Figure 4). At mid to high northern latitudes, the AO statistically explains 31% of the winter temperature variance [*Serreze et al.*, 2000] and about 40% of the winter temperature trends [*Thompson et al.*, 2000].

[10] To visualize the influence of the winter AO on land surface climate, Figure 5 correlates the AO index with the NCEP surface air temperature and precipitation for January–February–March or JFM (see methods below for a description of statistical techniques). Geostrophic balance and smoother zonal flow associated with positive AO polarity favors advection of warm, moist oceanic air deep into continental interiors, resulting in higher temperatures and increased precipitation. Positive AO polarity shifts the Atlantic storm tracks to the north, increasing precipitation north of 55°N latitudes in Eurasia and reducing precipitation south of 55°N. Positive AO polarity decreases the

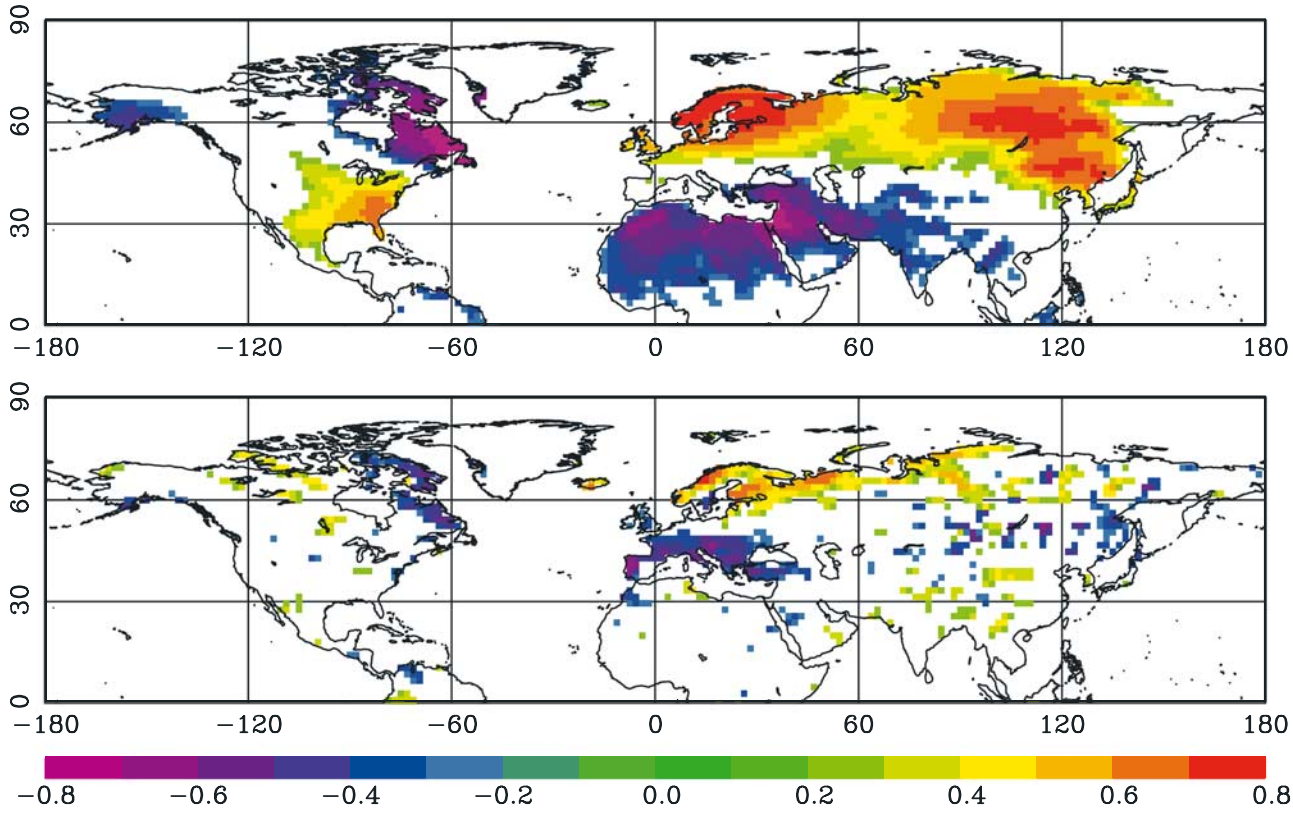

Figure 5. Statistically significant correlations between the average January–February–March (JFM) AO index and average JFM (a) surface air temperature and (b) precipitation from the NCEP reanalysis.

number of cold air outbreaks in central North America, resulting in positive temperature anomalies. Alaska and Northeast Canada show negative temperature and precipitation correlations, consistent with cold, dry airflow from the Arctic expected for positive AO polarity [*Thompson et al.*, 2000; *Thompson and Wallace*, 2000, 2001].

[11] We hypothesize that the trend in the winter AO can help explain the trends toward increased CO_2 amplitude, earlier springs, and higher NDVI. The winter AO and can statistically explain variability in the spring drawdown of atmospheric CO_2, although the exact mechanism is not well understood [*Russell and Wallace*, 2004]. Winter temperatures and the AO statistically explain most of the observed variability in spring phenophases in Europe [*D'Odorico et al.*, 2002; *Menzel*, 2003]. Lastly, positive AO polarity in winter is statistically associated with warmer temperatures and higher NDVI in spring in Eurasia [*Buermann et al.*, 2003]. We attempt to physically explain these relationships: a positive trend in the winter AO would increase winter temperatures, increasing winter respiration and the winter buildup of atmospheric CO_2. At the same time, warmer winter temperatures would advance the date of leaf-out, resulting in a greater CO_2 drawdown in spring and higher NDVI. Thus a trend in the winter AO can help explain observed advances in spring, higher NDVI, and increases in CO_2 amplitude.

[12] Climate memory is the mechanism by which the synoptic timescale AO might influence the timing of spring. Climate memory occurs where a relatively slowly changing component of the land system integrates the noisy climate input from the AO into a clear, persistent signal. Soil temperature, soil moisture, snow, and plant buds all have varying degrees of climate memory that could retain the climate signature of the winter AO well into spring and early summer, thus influencing terrestrial CO_2 fluxes and the timing of spring.

[13] Understanding the global carbon cycle is crucial to any long-term predictions on the climate effects of increased atmospheric CO_2. By linking the various trends described above to the winter AO trend, our research helps bridge independent lines of research in various scientific disciplines, advancing the science community toward a better understanding of the processes that drive variability in atmospheric CO_2.

2. Methods

[14] To test our hypothesis, we modeled photosynthesis and respiration using the Simple Biosphere model, Version 2 (SiB2) [*Sellers et al.*, 1996a, 1996b]. SiB2 separately tracks canopy, canopy air space, snow, and soil prognostic variables, accounting for the effects of snow cover, rainfall interception by the canopy, and aerodynamic turbulence. As the net terrestrial CO_2 flux, SiB2 calculates the Net Ecosystem Exchange (NEE):

$$NEE = R - GPP, \tag{1}$$

where R is total ecosystem respiration and GPP is Gross Primary Productivity or photosynthesis. A positive NEE indicates a net CO_2 flux into the atmosphere. To calculate GPP, SiB2 uses the *Farquhar et al.* [1980] photosynthesis model with a 10-min time step scaled to the canopy level [*Sellers et al.*, 1996a, 1996b] and the Ball-Berry-Collatz stomatal conductance model [*Ball*, 1988; *Collatz et al.*, 1991, 1992]. SiB2 is a balanced model, which means that respiration balances photosynthesis on an annual timescale. The respiration rate is not constant throughout the year, but is scaled based on the changing effects of soil temperature and moisture on respiration [*Denning et al.*, 1996; *Schaefer et al.*, 2002].

[15] As input weather data, we used the NCEP reanalysis from 1958–2002 [*Kalnay et al.*, 1996]. The NCEP reanalysis contains surface temperature, pressure, wind speed, precipitation, and radiation data every six hours on a Gaussian, 1.875° by 1.904° grid. Except for incident light, SiB2 linearly interpolated in time between data points. Incident light was scaled by the cosine of the solar zenith angle to conserve energy and assure no light falls on the canopy at night [*Zhang et al.*, 1996; *Schaefer et al.*, 2002].

[16] We modeled spring leaf-out using surface air temperature from the NCEP reanalysis. The timing of leaf-out (defined as the start of leaf development in the spring) depends primarily on temperature. After senescence in autumn, tree buds enter a state of dormancy. After sufficient chilling by exposure to cold temperatures, dormancy ends and the buds grow in response to warming in spring. When the buds have received a critical amount of cumulative thermal energy, they burst and leaf-out [*Cannell and Smith*, 1983, 1986; *Hunter and Lechowicz*, 1992; *Kramer*, 1994; *White et al.*, 1997; *Menzel and Fabian*, 1999; *Vaganov et al.*, 1999; *Beaubien and Freeland*, 2000; *Menzel*, 2000; *Los et al.*, 2001; *Chen and Pan*, 2002; *Menzel*, 2003].

[17] Available models of leaf-out are empirical and vary widely in complexity and in how they represent cumulative winter chilling and spring warming. We found that cumulative chilling did not vary significantly from year-to-year, so we chose a thermal time model, which performed well compared to other models and is adequate for predicting budburst [*Hunter and Lechowicz*, 1992; *Kramer*, 1994; *White et al.*, 1997; *Chuine*, 2000; *Tanja et al.*, 2003]. The thermal time model assumes a constant amount of chilling each year and represents bud warming as a cumulative sum of growing degree days from a fixed start date,

$$S = \sum_{\text{January 1}}^{S=S^*} GDD, \tag{2}$$

where S is the cumulative thermal forcing, S^* is the critical cumulative thermal forcing for leaf-out, and GDD is growing degree day. We used a start date of 1 January for S. Leaf-out occurs on the date when S exceeds S^*. GDD is defined as

$$GDD = \begin{cases} 0 & T < T_{base} \\ (T - T_{base})\Delta t & T \geq T_{base} \end{cases} \tag{3}$$

where T is surface air temperature from the NCEP reanalysis, T_{base} is the base temperature, and Δt is the

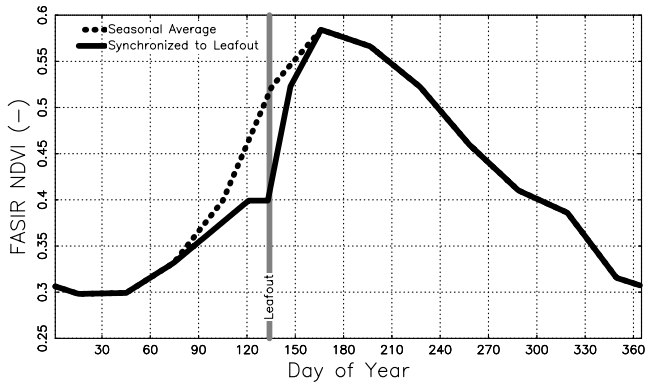

Figure 6. Interpolation of the FASIR NDVI data is synchronized with the estimated date of leaf-out. The dotted line is the seasonal average used in those years where we did not have observed NDVI. This sample is taken from (30°E, 55°N) for 1958.

model time step in days [*Cannell and Smith*, 1983; *Murray et al.*, 1989; *Chuine*, 2000].

[18] S^*, the critical cumulative thermal forcing for leaf-out, decreases exponentially with increased chilling in fall and winter,

$$S^* = a + be^{rC}, \tag{4}$$

where C is the cumulative annual chilling, a is the thermal time asymptote when the plant is fully chilled, b is the thermal response slope, and r is the chilling response slope ($r < 0$) [*Cannell and Smith*, 1983; *Murray et al.*, 1989; *Nikolov and Zeller*, 2003]. We calculated an S^* curve using empirical values of a, b, and r for 15 species of European trees and shrubs [*Murray et al.*, 1989; *Cannell and Smith*, 1983]. *Kaduk and Heimann* [1996] used NDVI data to estimate biome specific values of a, b, and r by ensuring the estimated leaf-out date corresponds to the date when the interpolated NDVI crosses a threshold value. We felt that S^* based on observed leaf-out is more suitable since the soil reflectivity can mask the relationship between NDVI and plant phenophases [*Chen and Pan*, 2002].

[19] We modeled chilling as a cumulative sum of chilling days,

$$C = \sum_{\text{November 1}}^{\text{April 30}} CD, \tag{5}$$

where CD is chilling day, defined as

$$CD = \begin{cases} 1 & T_d < T_{base} \\ 0 & T_d \geq T_{base} \end{cases}, \tag{6}$$

where T_d is the daily average surface air temperature from the NCEP reanalysis [*Cannell and Smith*, 1983, 1986; *Hunter and Lechowicz*, 1992; *Murray et al.*, 1989; *Kaduk and Heimann*, 1996; *Chuine*, 2000; *Nikolov and Zeller*, 2003]. To calculate C, we assumed a start date of 1 November [*Murray et al.*, 1989; *Cannell and Smith*, 1983] and a stop date of 30 April (we found longer time periods did not change S^*). Annual chilling based on the NCEP surface air temperature did not vary significantly from year to year, so we calculated S^* assuming a 45-year average of C. S^* does not show significant spatial variability: at high latitudes, the chilling is very deep such that S^* lies near its asymptotic limit of 62°C day. At mid latitudes, S* increases sharply and near the equator, where C approaches zero, we placed an upper limit on S^* of 200 °C day.

[20] The choice of T_{base} is more important at high latitudes than in the temperate regions. In temperate regions (south of 55°N) T_{base} and S^* compensate for each other: lowering T_{base} lowers C and increases S^* such that leaf-out occurs at nearly the same time. For vast regions at high latitudes, however, S^* lies near its asymptotic limit, and is essentially independent of C and thus T_{base}. However, S, GDD, and leaf-out still depend on T_{base}. For consistency, we used the T_{base} of 5°C used by *Murray et al.* [1989] and *Cannell and Smith* [1983] to empirically estimate a, b, and r.

[21] The modeled GPP depends on the absorbed fraction of Photosynthetically Active Radiation (fPAR), which we estimated from monthly composite maps of NDVI. The monthly composite maps contain the maximum observed NDVI values during the month for each pixel, adjusted for missing data, satellite orbit drift, differing instrument calibrations, sensor degradation, and volcanic aerosols. We used Fourier-Adjustment, Solar zenith angle corrected, Interpolated Reconstructed (FASIR) NDVI data set, version 3.04b [*Sellers et al.*, 1994; *Los*, 1998; *Los et al.*, 2000]. Daily values of NDVI are interpolated from monthly composite values, which are arbitrarily assigned to the middle of the month (the actual observation time can be anytime in the month). The NDVI data set covered only 1983–1998. In those years for which we did not have NDVI data (1958–1982 and 1999–2002), we used an average seasonal cycle of FASIR NDVI.

[22] An average seasonal cycle for NDVI would produce the same values of fPAR each year, regardless of the timing of spring, so we synchronized the NDVI interpolation to our estimated date of leaf-out. We assumed the maximum NDVI for the month prior to leaf-out occurred at the end of the month. For the month of leaf-out, the NDVI stays constant at the previous month's value until the estimated date of leaf-out. After leaf-out, we interpolate to that month's NDVI value over a 2-week green-up period or the end of the month, whichever comes first.

[23] Figure 6 illustrates the resulting interpolated NDVI values for a randomly chosen pixel at midlatitudes (30°E, 55°N) for 1958. The synchronized NDVI curve is not as smooth as interpolating from midmonth values, especially if leaf-out occurs near the end of the month. Using the actual dates for each NDVI value [*White et al.*, 1997] or more sophisticated curve fitting techniques [*Potter et al.*, 1999; *Chen and Pan*, 2002; *Shabanov et al.*, 2002] would result in smoother NDVI curves.

[24] We related the AO to leaf-out, CO_2 fluxes, and other variables using correlations, regressions, and congruent trend fractions. We started with global maps of monthly

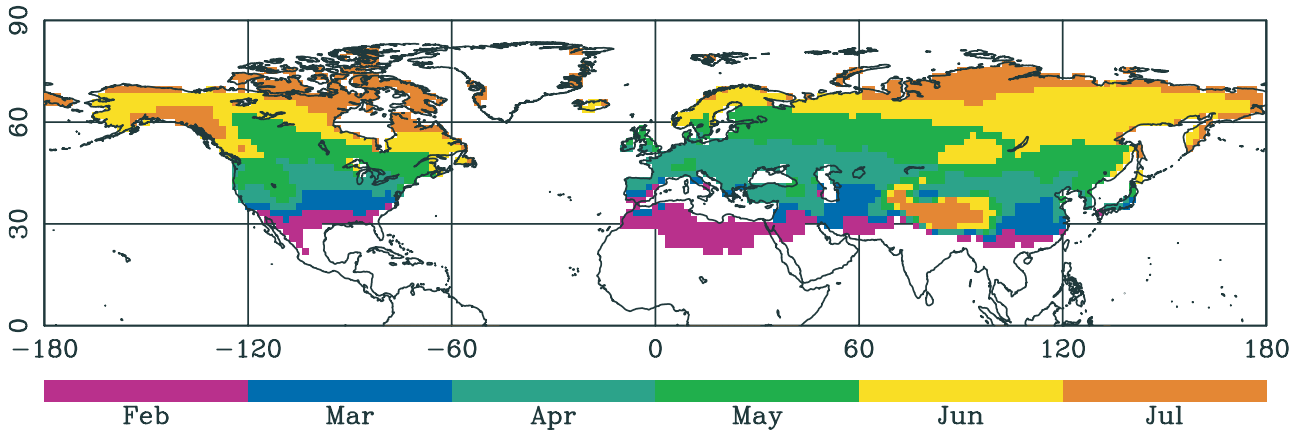

Figure 7. Modeled mean dates of leaf-out (month). Omitting January mean values leaves a southern margin near 30°N latitude south of which leaf-out is undefined.

mean terrestrial CO_2 fluxes, temperature, and other variables, and annual maps of leaf-out date. We first averaged over a particular season or portion of the year, removed long-term, linear trends, and lastly removed the seasonal mean. For example, for the AO index, we first averaged over January–February–March (JFM), then removed the long-term, JFM trend, and lastly removed the long-term, JFM mean. For leaf-out, which are annual values, we removed the long-term trends and then the long-term means. This resulted in time series of detrended, annual anomalies from which we calculated regressions, standard deviations, and other statistics. Detrending is required, otherwise, regressions and correlations would simply reflect the ratio of the trends rather than a statistical correlation of anomalies. We omitted trends, correlations, regressions, and congruent trend fractions failing a single-tail student T-test at 95% significance. The degrees of freedom for the T-test were based on the number of years in the simulation (45 years).

[25] Congruent trend fractions quantify how a trend in one variable can statistically explain trends in other variables. The congruent trend fraction, f_C, is the fraction of the trend in variable y statistically explained by a trend in variable x,

$$f_C = r\frac{t_x}{t_y}, \tag{7}$$

where r is the regression coefficient between x and y, t_y is the trend in y, and t_x is the trend in x [*Thompson et al.*, 2000]. The strength of the correlation between x and y determines how much of the trend in y is statistically explained by the trend in x. When x and y do not correlate, $r = 0$, $f_C = 0$, and the trend in x does not statistically explain the trend in y. When the correlation between x and y approaches ±1, r approaches t_x/t_y, $f_C = 1$, and the trend in y is entirely explained by the trend in x. Values of f_C less than zero or greater than one indicate that a trend in some another variable is also influencing the trend in y. Like all statistical relationships, whether x causes y or y causes x must be justified by physical argument. The congruent trend fraction is statistically significant only when r, t_x, and t_y are all statistically significant.

3. Results

3.1. Winter AO and Leaf-out

[26] Figure 7 shows the 45-year mean dates of simulated leaf-out. We omitted all January mean values to form a southern margin at about 30°N. We assumed that south of this southern margin, leaf-out is undefined because other mechanisms, such as seasonal rainfall, drive transitions between seasons.

[27] Estimated leaf-out dates compare fairly well with available regional observations. As expected from a model based on temperature, predicted leaf-out matches spring in Europe estimated from observed temperatures [*Jaagus et al.*, 2003]. Predicted leaf-out occurs, on average, about one week earlier than observed birch leaf-out in Europe [*Ahas et al.*, 2002], which represents fair agreement since the average S^* curve represents many species that typically leaf-out over a period of several weeks.

[28] The leaf-out model is based only on NCEP surface air temperature, independent of the NDVI used as input to SiB, allowing us to compare our estimated leaf-out with dates derived from NDVI. Our estimated leaf-out is 2–4 weeks earlier than leaf-out for the continental United States estimated from NDVI [*White et al.*, 1997]. However, leaf-out estimated from NDVI is very uncertain and depends strongly on the threshold used to define the start of greening in the spring. The *White et al.* [1997] threshold arbitrarily represents the midpoint between annual minimum and maximum NDVI. A slightly lower threshold that better represents the start of spring greening would advance the leaf-out dates estimated by *White et al.* [1997] by several weeks, bringing them into much closer agreement with our estimated leaf-out dates. Overall, our estimated leaf-out dates are slightly earlier than observed, but reasonable.

[29] The largest source of uncertainty in our leaf-out model is the extreme scarcity of the phenological observa-

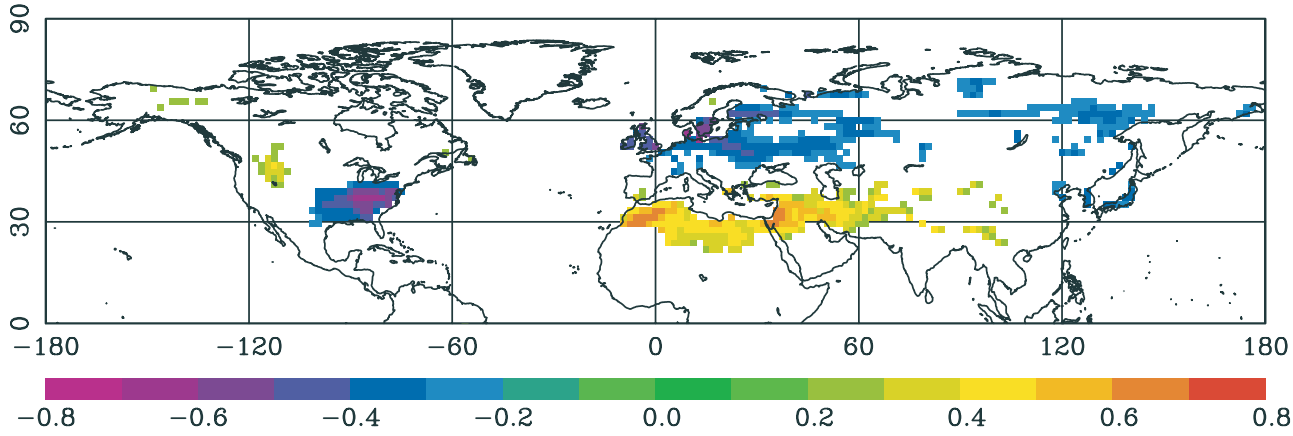

Figure 8. Statistically significant correlations between the JFM AO index and the modeled date of leaf-out.

tions needed to construct the average S^* curve. The literature references hundreds of phenological studies, but most focus on one or two species at a specific location, making it difficult to construct suitable regional or global S^* curves. Our average S^* curve is based on temperate tree and shrub species from Europe and may not adequately represent leaf-out in other regions. Our modeled leaf-out dates at high latitudes, where S^* becomes independent of T_{base}, are particularly uncertain. A global leaf-out model needs global data sets of observed leaf-out for many species.

[30] Leaf-out correlates most strongly with the winter (JFM) AO in those regions where leaf-out occurs before June: Eurasia, North Africa, and the eastern United States (Figure 8). In Eurasia and eastern United States, positive AO polarity in winter produces positive temperature anomalies, earlier leaf-out, and negative correlations. In North Africa, positive AO polarity in winter produces negative temperature anomalies, later leaf-out, and positive correlations.

[31] The JFM AO does not correlate well with leaf-out at high latitudes where leaf-out typically occurs in June or July, such as northern Siberia. At such high latitudes, the winter AO influences temperature, but the JFM temperatures are too cold to influence the thermal sum, so temperatures in April and May, after the breakdown of the winter polar vortex and weakening of the AO, determine the timing of leaf-out. Correlations are weak in regions where the JFM AO influences both precipitation and temperature, such as northeast Canada and Scandinavia. Generally, leaf-out occurs just after the snowmelts and snowmelt depends on spring temperatures and cumulative winter precipitation. In northeast Canada, colder temperatures associated with positive AO polarity compensate for decreased precipitation, resulting in no AO influence on snowmelt, and thus leaf-out. In Scandinavia, increased precipitation for positive AO polarity compensates for increased temperatures, also resulting in little AO influence on snowmelt [*Schaefer et al.*, 2004]. Lastly, in Alaska and parts of North America, the El Niño-Southern Oscillation (ENSO), in addition to the winter AO, can influence winter temperatures and precipitation, and thus the timing of leaf-out [*Cutforth et al.*, 1999; *Beaubien and Freeland*, 2000].

[32] The strength of the correlations between leaf-out and the JFM AO depend entirely on the climate memory

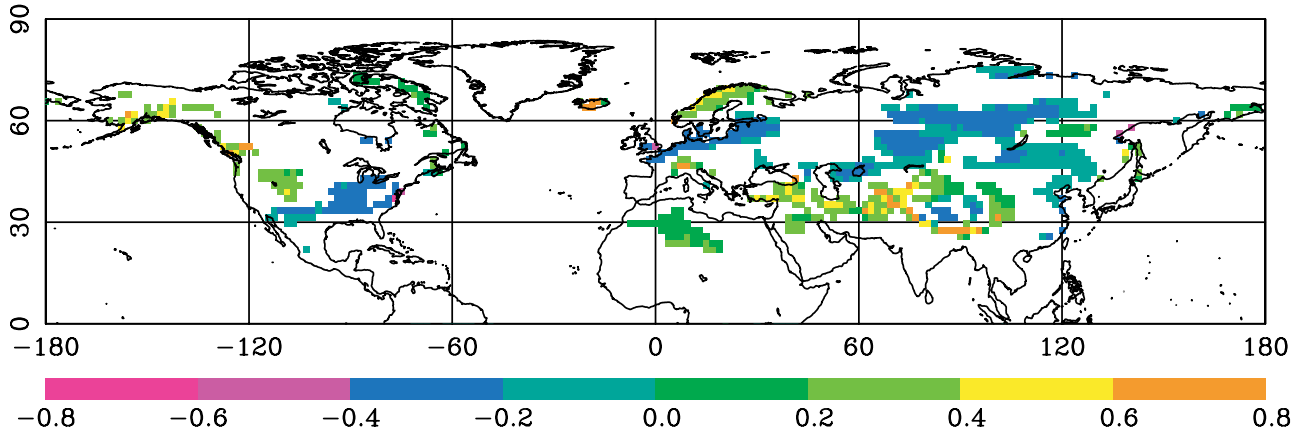

Figure 9. Statistically significant trends in the modeled date of leaf-out (day yr^{-1}).

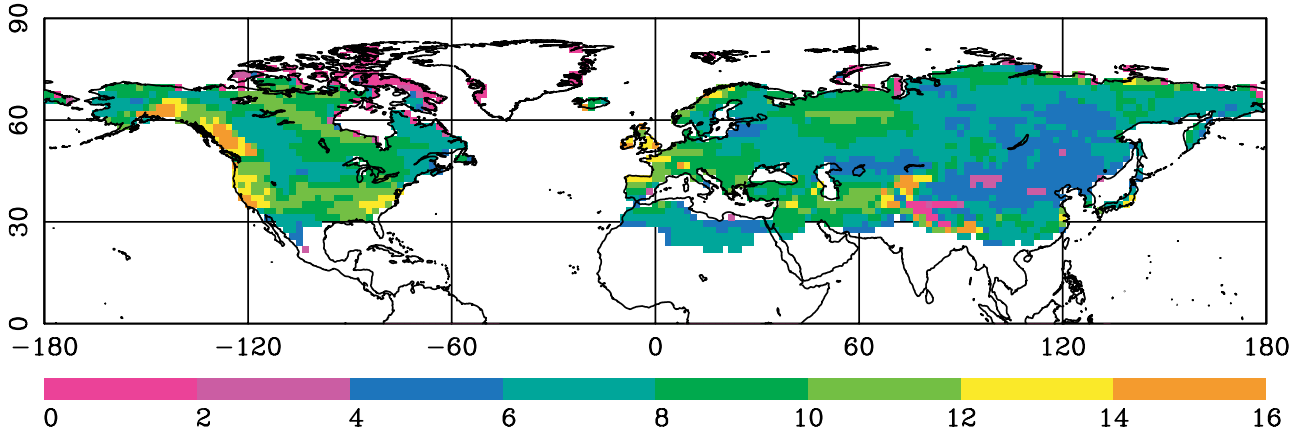

Figure 10. Standard deviation of the modeled date of leaf-out (day).

of the leaf-out model. For example, lowering the T_{base} from 5°C to 0°C increases the climate memory of the leaf-out model by increasing both S^* and the number of days included in the thermal sum. This increased climate memory allows the JFM AO to influence the thermal sum in high latitude regions where leaf-out typically occurs in June or July, producing a correlation pattern as strong as seen in Figure 5a, but of opposite sign (not shown). Leaf-out models that use soil rather than air temperature [*White et al.*, 1997; *Tanja et al.*, 2003] correlate more strongly with the JFM AO than those based on air temperature because the heat capacity of soil is much greater than that of air, resulting in a greater thermal inertia and a longer climate memory. Using the prognostic canopy air space temperature from SiB2, which has a slightly longer climate memory than the NCEP surface air temperature, also produces stronger correlations with the JFM AO (not shown). Although the spatial pattern does not change, any choice of temperature, T_{base} and S^* that increases the climate memory of the leaf-out model will strengthen the correlations between estimated leaf-out and the winter AO.

[33] Simulated trends (Figure 9) indicate that leaf-out has advanced between 1958 and 2002 (positive trends indicate delay and negative trends indicate advance). The magnitude and locations of the modeled trends are consistent with observed trends in Europe [*Menzel and Fabian*, 1999; *Menzel*, 2000; *Ahas et al.*, 2002; *Scheifinger et al.*, 2002; *Menzel*, 2003] and North America [*Keyser et al.*, 2000; *Schwartz and Reiter*, 2000]. The strongest trends occur in those regions that experience increased temperatures and neutral or decreased precipitation associated with a positive trend in the AO. Positive trends (later springs) along the southern margin in Africa, the Middle East, and Himalaya are consistent with lower temperatures associated with the AO. The trends toward later springs in far northern Europe and the North American Rockies through to Alaska result from negative temperature trends in May, unrelated to the trend in the winter AO.

[34] Only regions of relatively low variability in the date of leaf-out show statistically significant trends. Figure 10 indicates that trends are only statistically significant when the standard deviation is less than roughly 6–8 days. This highlights the difficulty in identifying statistically signifi-

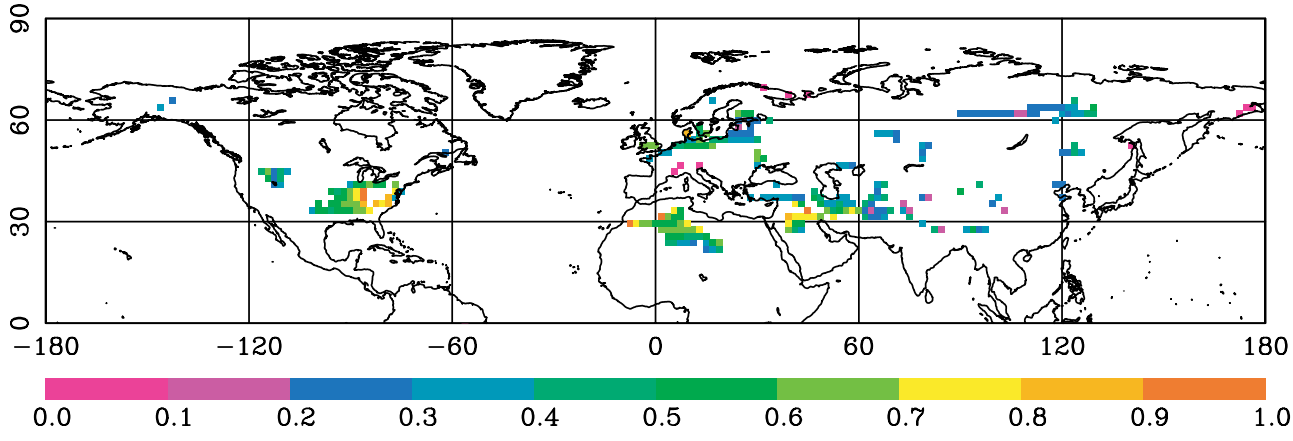

Figure 11. Statistically significant fractions of leaf-out trends statistically explained by the JFM AO trend.

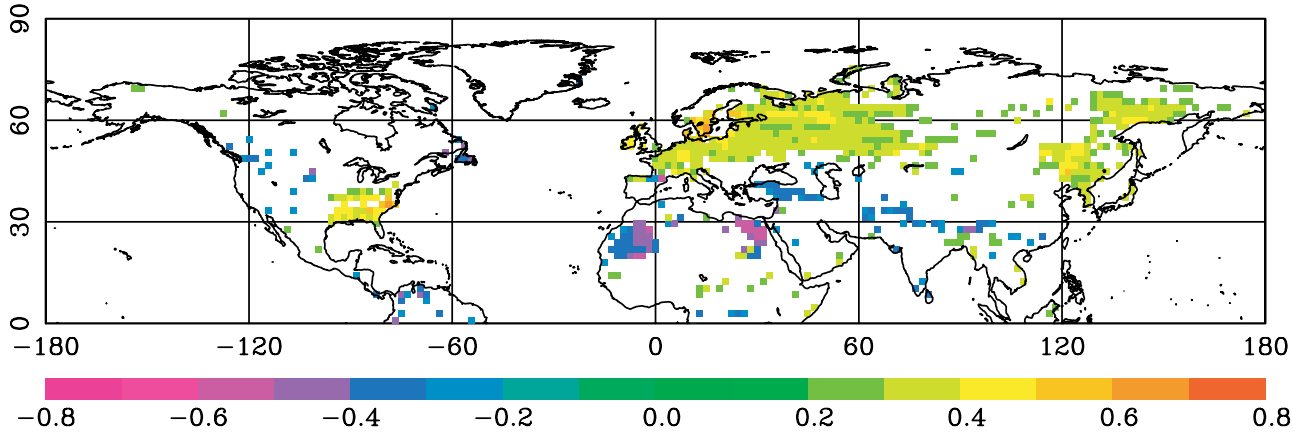

Figure 12. Statistically significant correlations between the total modeled GPP from January through June and the JFM AO index.

cant trends from a noisy signal. Other regions in the high northern latitudes may, in fact, show trends toward earlier springs, but our 45-year simulation is too short to detect them.

[35] The trend in the winter AO can statistically explain a large fraction of simulated leaf-out trends in the eastern United States and northern Europe (Figure 11). The congruent trend fractions in Figure 11 are statistically significant only where r, t_{ao}, and t_{spring} are all statistically significant (the overlap between Figures 8 and 9). In the eastern United States, the AO influence on leaf-out trends varies between 40 and 70%. In northern Europe, the AO influence on leaf-out varies between 20 and 50%. The congruent trend fractions in Siberia and Asia are too scattered to form any strong conclusions.

3.2. Winter AO and GPP

[36] By influencing the timing of spring, the winter AO influences the start of the growing season. Earlier springs associated with a trend toward positive AO polarity in winter result in longer growing seasons, greater total GPP, and a greater drawdown in atmospheric CO_2. The average JFM AO index positively correlates with total simulated GPP from January through June (Jan-Jun) where the winter AO most strongly influences winter temperature, and thus the timing of spring (Figure 12). Using total annual GPP (full growing season) produces a similar spatial pattern (not shown), but much weaker correlations because the JFM AO influences the start, but not the end of the growing season. This indicates the drawdown period for CO_2 in spring and early summer is modulated by the winter AO through its influence on the timing of spring, consistent with results of *Russell and Wallace* [2004].

[37] The Jan-Jun GPP trends show strong regional differences, only some of which we can attribute to the AO (Figure 13). Large positive trends in western North America, for example, result from a long-term trend in annual precipitation unrelated to the AO. The precipitation trends also produce positive respiration trends in the same region which cancel the GPP trends, resulting in no trend in NEE. The fraction of Jan-Jun GPP trends linearly congruent with the JFM AO trend (Figure 14) indicate that the AO

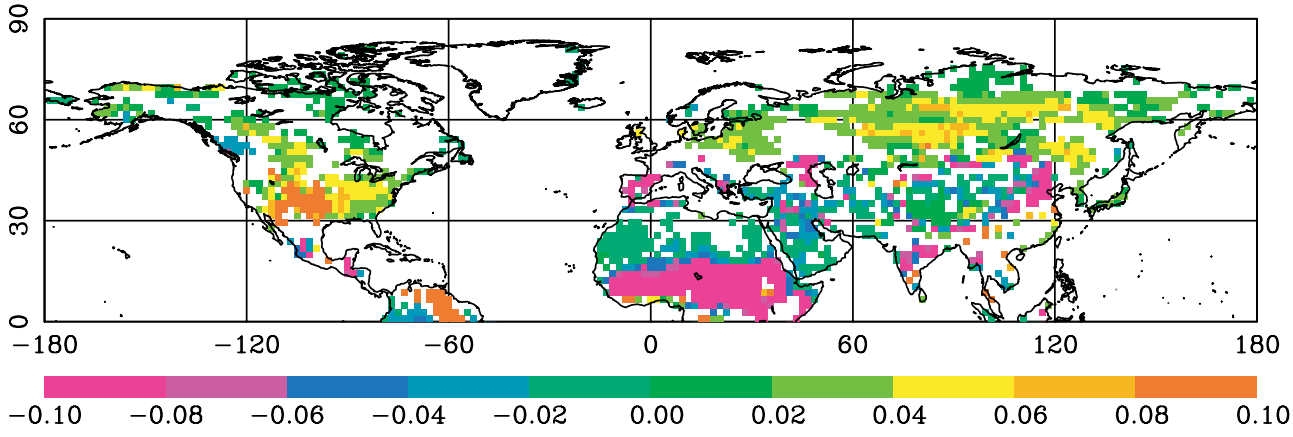

Figure 13. Statistically significant trends in total modeled GPP from January through June (μmoles m^{-2} s^{-1} yr^{-1}).

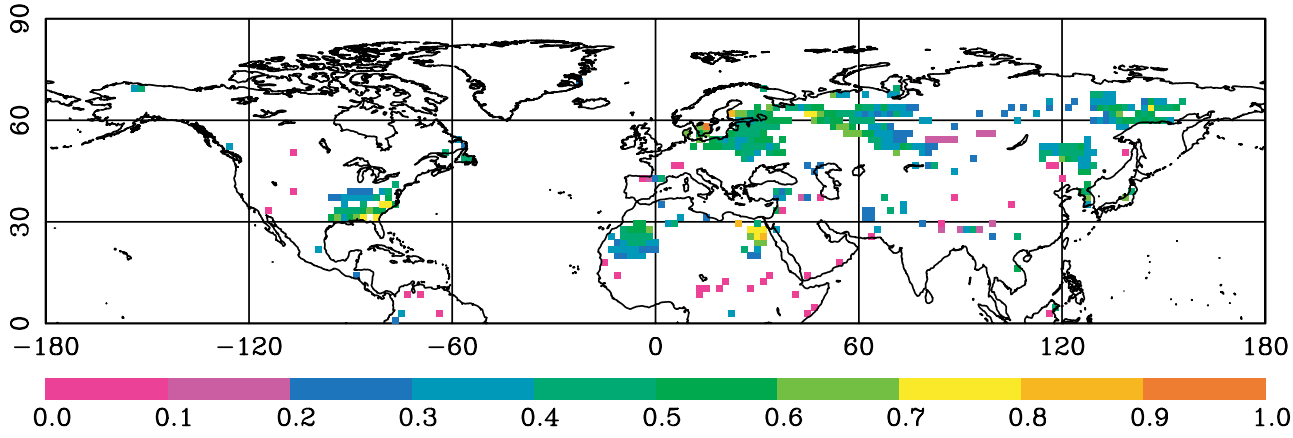

Figure 14. Statistically significant fractions of trends in total modeled GPP from January through June statistically explained by the JFM AO trend.

statistically explains 30–70% of the GPP trends in those regions where the AO exerts a strong influence on the timing of spring.

[38] In addition to the timing of spring, the winter AO can influence GPP through temperature control of enzyme kinetics within the leaf chloroplasts, although the magnitude of the effect shows strong spatial variability. For example, regressions between the March AO index and simulated March GPP are statistically significant, but vary by a factor of 10 or more (Figure 15). In March, much of Northern Hemisphere still lies in the grip of winter. Needleleaf, evergreen trees can photosynthesize even in winter [*Zimov et al.*, 1999], so SiB2 estimates a very small, but non-zero GPP that correlates well with the AO. Regression coefficients clearly indicate that the magnitude of the direct AO influence on enzyme kinetics is very small except in those areas where spring occurs in March.

3.3. Winter AO and Respiration

[39] Correlations between the January AO index and January soil respiration (Figure 16) show strong positive correlations in Eurasia and North America where the AO most strongly influences temperature. Respiration increases exponentially with soil temperature, so positive temperature anomalies associated with positive AO polarity result in positive respiration anomalies. Correlations with the February and March AO indices show similar patterns (not shown). This indicates that temperature anomalies associated with the winter AO influence the winter buildup of atmospheric CO_2.

[40] The climate memory of the soil allows the winter AO temperature signal to persist for many months. Lagged correlations between the January AO index and soil temperatures in Siberia (Figure 17) peak later at deeper depths as the AO-induced soil temperature anomaly propagates into the soil. The surface soil layers are more responsive to atmospheric temperature forcing, so the strong correlations drop off within 3 months. The correlations for the middle soil layers increase as the AO driven temperature anomaly penetrates deeper into the soil. The lagged correlations persist longer at deeper depths because in SiB, soil layer thickness increases with depth and deeper layers have greater heat capacity. After 4 months, the winter AO temperature anomaly has reached the deepest soil layer in

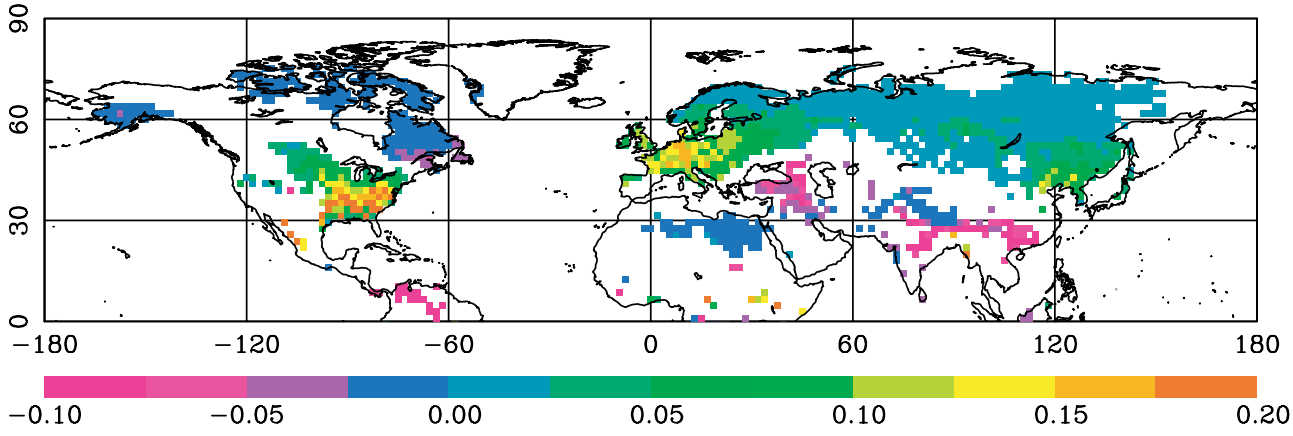

Figure 15. Statistically significant regression coefficients between the March AO and modeled March GPP (μmole m^{-2} s^{-1} AO $unit^{-1}$).

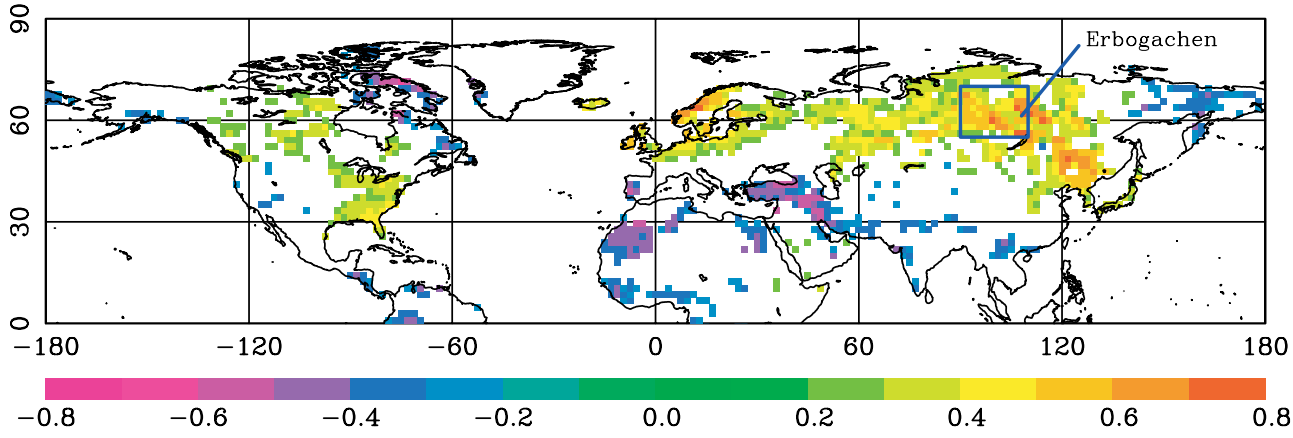

Figure 16. Statistically significant correlations between the January AO index and modeled January respiration. The blue box is the area used in Figures 17 and 19. Soil temperatures at Erbogachen are shown in Figure 18.

SiB (4 m). Although no longer felt at the surface, the AO soil temperature anomaly persists at depth for many months. Correlations using December, February, or March AO indices give similar results (not shown).

[41] Lagged correlations between observed soil temperatures at Erbogachen in Northern Russia (108°E, 61°N) and the January AO index also peak later at deeper depths (Figure 18). The data for Erbogachen was extracted from a data set of monthly average soil temperatures as a function of depth collected at 103 stations scattered across Russia and Siberia between 1900 and 1990 [*Barry et al.*, 2001]. Observations at Erbogachen covered a period of 36 years (1955–1990). The correlations at Erbogachen were generally weaker than those using modeled temperature and dropped off faster, indicating differences between modeled and actual soil thermal conductivity and heat capacity. Three of the five stations located within the region used to calculate Figure 17 and many of the other stations in western Russia showed lagged correlations similar to Figures 17 and 18.

[42] Both the observed and modeled soil temperatures show secondary correlation peaks in late summer and early autumn, although the secondary peak varies in strength from station to station and is not always statistically significant. The thermal inertia of the deep soil causes the winter AO thermal anomaly to migrate back to the surface as the vertical temperature gradients switch between winter and summer. The deep soil temperature stays relatively constant over time while the surface soil is colder than deep soil in winter and warmer in summer. Warmer deep soil in summer due to positive AO polarity the previous winter decreases the vertical temperature gradient, slowing the downward migration of thermal energy and causing positive temperature anomalies in shallow soil layers in late summer.

[43] SiB assumes root density, and thus soil carbon, decreases exponentially with depth [*Jackson et al.*, 1996], so the AO influence on respiration decreases with time as the AO-induced temperature anomaly sinks below the soil carbon. Lagged correlations between the January AO index and modeled soil respiration in Siberia (Figure 19) drop off completely by May because most of the soil carbon lies near the surface (95% in the top 1 m of soil). Comparing Figures 17 and 19 indicates respiration correlations closely follow temperature correlations for the top three soil layers, which contain the bulk of the soil carbon. Although winter AO temperature anomalies may persist at depth well into summer, the effect on respiration is limited to spring and early summer.

3.4. AO and NEE

[44] Figure 20 shows the long-term (45-year) mean of the total zonal NEE for winter (December–January–February or DJF), spring (March-April-May or MAM), summer (June–July–August or JJA), and fall (September–October–November or SON). From autumn through winter, GPP effectively shuts down, and R determines NEE. In spring, large GPP associated with spring greening dominates NEE at the lower latitudes while the higher latitudes still

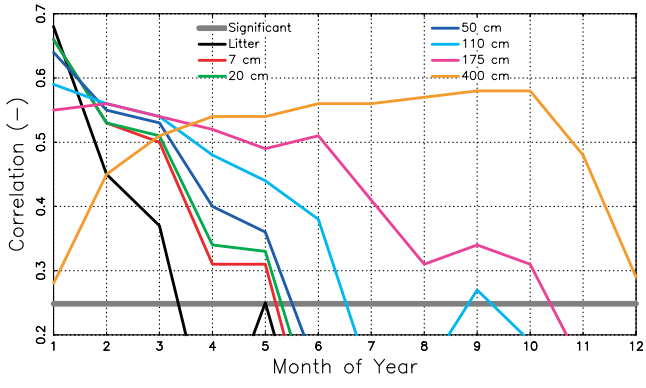

Figure 17. Lagged correlations between the January AO index and the area average of modeled soil temperature in Siberia (blue box in Figure 16). The thick gray line denotes statistical significance.

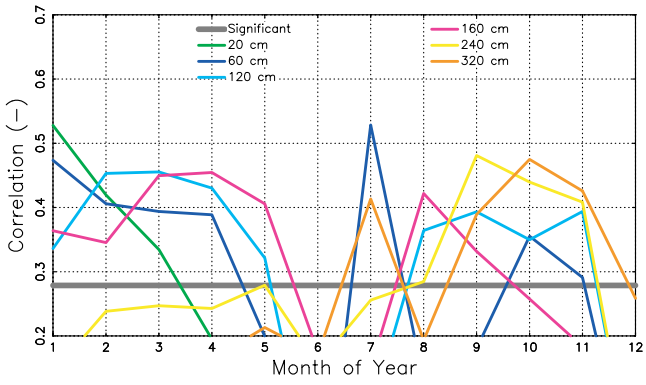

Figure 18. Lagged correlations between the January AO index and observed soil temperature at Erbogachen in Siberia (see Figure 16) from 1955–1990 (36 years). The thick gray line denotes statistical significance.

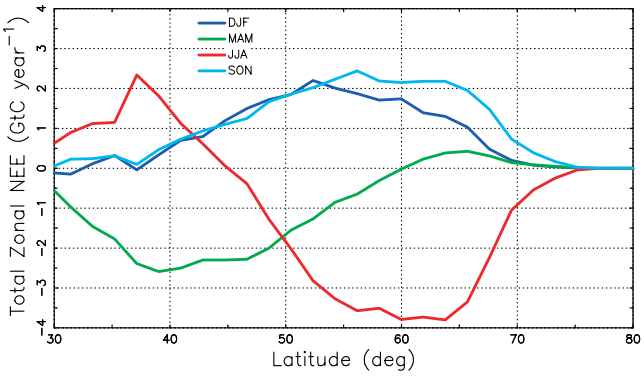

Figure 20. Long-term (45-year) mean of modeled total zonal NEE (GtC yr^{-1}) for winter (DJF), spring (MAM), summer (JJA), and fall (SON).

show winter respiration. By summer, the spring green wave has moved north to the higher latitudes while at the lower latitudes spring has passed and summer respiration dominates.

[45] Correlations between the AO and NEE change from positive to negative in the spring as the AO influence on GPP exceeds its influence on respiration (Figure 21). Several weeks before leaf-out, evergreen trees become warm enough to begin photosynthesis, producing a green wave of increased GPP moving northward about 2–3 weeks in advance of leaf-out. In front of the green wave, respiration exceeds GPP (positive NEE) while behind the wave GPP exceeds respiration (negative NEE). Thus in front of the green wave, we see positive correlations between the AO and NEE, indicating increased respiration due to warmer temperatures. Behind the green wave we see negative correlations indicating increased GPP due to warmer temperatures and earlier spring. This shifting influence might explain why previous studies [*Schaefer et al.*, 2002; *Reichenau and Esser*, 2003] did not find a strong link between NEE and the AO: the location of highest AO influence on NEE moves northward with spring.

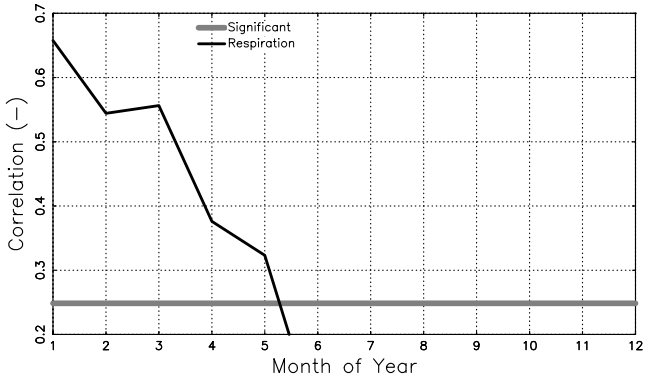

Figure 19. Lagged correlations between the January AO index and area average of modeled respiration in Siberia (blue box in Figure 16). The thick gray line denotes statistical significance.

[46] Our simulation shows seasonally asymmetric NEE trends (Figure 22), which can partially explain the trend toward increased CO_2 amplitudes. DJF shows increased NEE north of 55°N and decreased NEE south of 55°N owing to changes in respiration consistent with temperature trends associated with the winter AO. The MAM trends result from increased GPP consistent with earlier springs and warmer temperatures associated with the winter AO trend. The DJF trends are weaker than the MAM trends, primarily owing to the much lower temperatures in winter compared to spring. This is consistent with the amplitude trend at Barrow, which results primarily from a decrease in the minimum CO_2 (increased spring drawdown). The DJF and MAM trends indicate that a trend toward positive AO polarity in winter can increase both winter build up and spring drawdown of atmospheric CO_2, resulting in increased CO_2 amplitudes.

[47] Summer (JJA) shows large positive trends in NEE due almost entirely to trends toward increased respiration in August associated with positive trends in temperature. Respiration increases exponentially with temperature. Although the temperature trends in summer are actually smaller than winter, the effect is stronger owing to the much warmer temperatures of summer relative to winter.

[48] The trend in the August AO does not appear to drive the trend in summer NEE. As shown in Figure 23, the August AO exerts a fairly strong influence on NEE in North America with a weaker influence in Europe. Also, the August AO index shows a statistically significant trend toward positive polarity. However, the August trends in NEE all lie in Eurasia (Figure 24). If the August AO trend were really the driving force behind the temperature trends, we should also see NEE trends in North America, where the AO influence is stronger. Although the AO may amplify the NEE trends in Europe, the August temperature and associated respiration trends probably result from some mechanism other than the AO.

[49] Using a model that estimates net annual sources and sinks would produce similar results because the seasonally

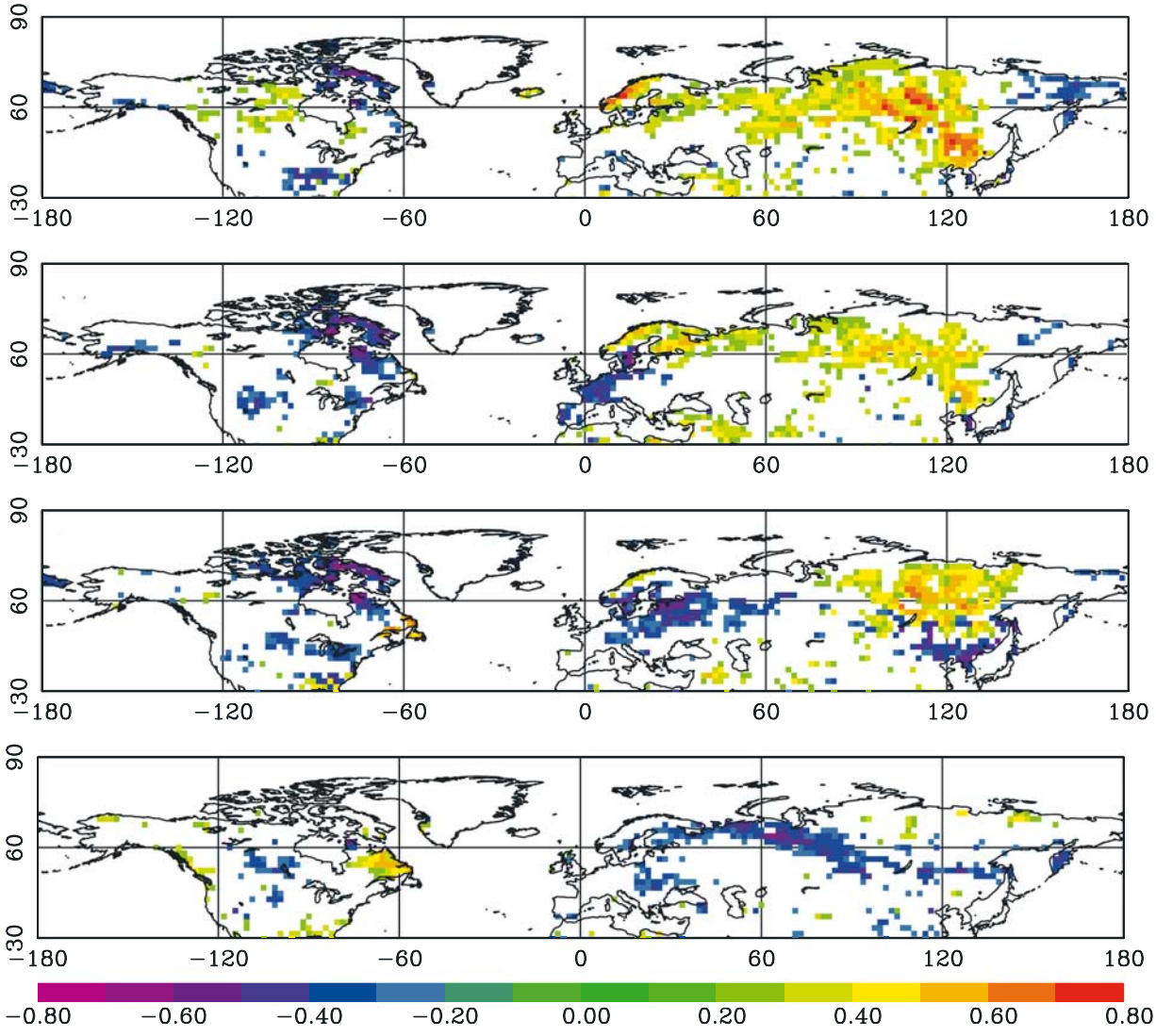

Figure 21. Statistically significant correlations between the AO index and modeled NEE for (a) January, (b) February, (c) March, and (d) April.

asymmetric trends in NEE are driven by seasonally asymmetric trends in climate. SiB2 is a balanced model such that NEE equals zero on an annual timescale, so all the zonal trends in Figure 22 sum to zero. We know however, that the terrestrial biosphere is a net carbon sink which is increasing with time [e.g., *Sarmiento and Gruber*, 2002]. Assuming no seasonal dependence, a trend in the annual carbon sink would shift the curves in Figure 22 downward, but seasonally asymmetric trends in temperature would still produce seasonally asymmetric trends in NEE.

[50] Our results support the *Zimov et al.* [1996] and *Wu and Lynch* [2000] theory that seasonally asymmetric fluxes can change the amplitude of the CO_2 seasonal cycle, even if the annual total fluxes are unchanged. Our results do not support the theory that shifts in the timing of peak photosynthesis in spring can explain the amplitude trends, as proposed by *Chapin et al.* [1996] and *Stone et al.* [2002]. We found that the timing of maximum and minimum NEE

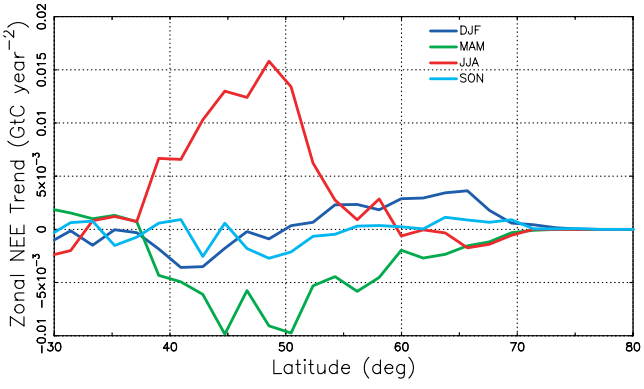

Figure 22. Trends in modeled total zonal NEE (GtC yr^{-2}) for winter (DJF), spring (MAM), summer (JJA), and fall (SON).

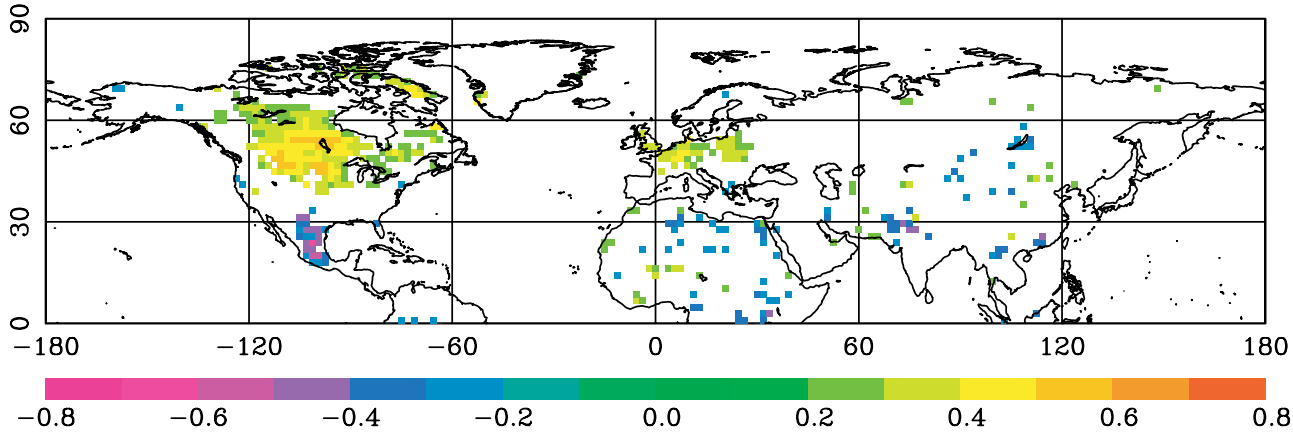

Figure 23. Statistically significant correlations between the August AO index and modeled August NEE.

showed little, if any, interannual variability and few statistically significant trends. Although the start of the spring drawdown and the magnitude of peak GPP show considerable interannual variability and statistically significant trends, the timing of peak GPP does not. Since we did not include a transport model in our simulations, our results neither support nor refute the shifting source region theory proposed by *Dargaville et al.* [2000]. A more definitive evaluation of both the asymmetric flux theory and the shifting source region theory requires a coupling of our simulated fluxes to a global transport model for direct comparison to observed CO_2 concentrations.

3.5. AO and NDVI

[51] We found the NDVI time record too short to form any firm conclusion on the relationship between the AO and NDVI trends. The locations of the NDVI trends in Eurasia and the eastern United State are consistent with the modeled trends in leaf-out. The spring NDVI positively correlates with the winter AO [*Los et al.*, 2001], indicating that positive temperature anomalies result in larger values of NDVI. In addition, the spring NDVI strongly correlates with the date of leaf-out (not shown), indicating that earlier springs result in larger values of NDVI. These strong correlations suggest a link between the winter AO, leaf-out, and NDVI trends. However, our analysis was inconclusive because the 17-year NDVI time record is too short to estimate statistically significant trends in either leaf-out or the JFM AO.

4. Conclusions and Discussion

[52] We found that terrestrial ecosystems have sufficient climate memory to integrate the noisy AO signal over time to control the transition from winter to spring. In general, positive AO polarity during winter results in positive winter temperature anomalies and earlier springs. Our modeled leaf-out values and trends are consistent with observations. The AO shows a statistically significant influence on leaf-out trends in the eastern United States and northern Europe.

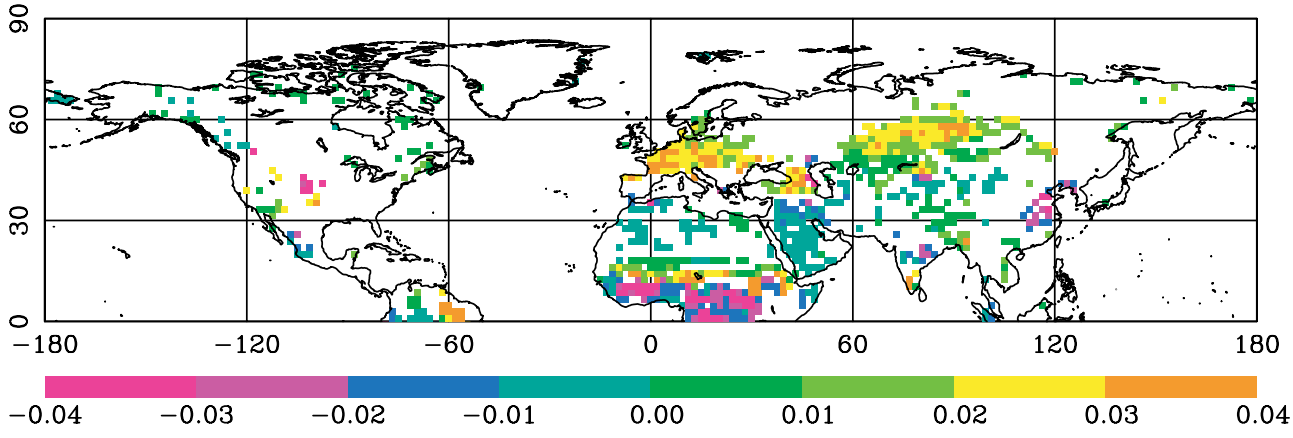

Figure 24. Statistically significant trends in modeled August NEE (μmoles m^{-2} s^{-1} yr^{-1}).

[53] Positive AO polarity increases winter respiration and spring GPP, contributing to both winter buildup and spring drawdown of atmospheric CO_2. The soil retains the temperature signal of the winter AO for many months, influencing respiration fluxes well into spring. Increased temperatures associated with positive AO polarity in winter results in a greater CO_2 drawdown due to earlier springs and longer growing seasons.

[54] Seasonally asymmetric trends in NEE are consistent with the observed trend toward increased seasonal amplitudes in atmospheric CO_2. Trends toward increased GPP in spring and respiration in August can result in a trend toward larger CO_2 seasonal amplitudes, even though the annual net flux does not change. The trends toward increased respiration in winter and GPP in spring can be partially explained by the AO influence on the timing of spring. The August respiration trends are probably not due to the positive trend in the August AO.

[55] Climate memory allows variability and trends to cut across timescales. The climate memory of terrestrial ecosystems allows the synoptic timescale variability of the winter AO to influence the timing of leaf-out in spring and the seasonality of NEE. Consequently, to fully explain observed trends in seasonal dynamics, such as earlier springs or longer growing seasons, we must examine processes at all timescales. Climate phenomena operating on multiple timescales can influence the timing of spring. For example, the AO, which operates on a synoptic timescale, and ENSO, which operates on an interannual timescale, might jointly influence observed leaf-out variability and trends in North America.

[56] Our analysis indicates that changes in circulation rather than direct global warming can partially explain the observed springtime trends. The winter AO trend itself may result from global warming, stratospheric ozone loss, or both, although the exact mechanism is not fully understood [*Hartmann et al.*, 2000; *Hoerling et al.*, 2001; *Shindell et al.*, 1999]. Alternatively, the winter AO trend may result from natural variability of the atmosphere on a century timescale. Although our modeled spring trends generally agree with observations, the observed trends are no larger than interdecadal variability [*White et al.*, 1999; *Hartley and Robinson*, 2000; *Serreze et al.*, 2000]. Consequently, observed trends toward earlier spring may reflect long-term climate variability rather than climate change.

[57] **Acknowledgments.** We thank the National Oceanic and Atmospheric Administration, Climate Monitoring and Diagnostics Laboratory, Boulder, Colorado for supplying observations of CO_2 concentration. We thank David Thompson of the Atmospherics Sciences Department, Colorado State University for valuable advice and insight regarding our analysis of the Arctic Oscillation. This research was funded by NASA grants NCC5-621 and NNG04GH53G. Partial funding was also provided through the Monfort Professor Award from Colorado State University.

References

Ahas, R., A. Aasa, A. Menzel, V. G. Fedotova, and H. Scheifinger (2002), Changes in European spring phenology, *Int. J. Climatol.*, *22*, 1727–1738.

Angert, A., S. Biraud, C. Bonfils, W. Buermann, and I. Fung (2004), CO_2 seasonality indicates origins of post-Pinatubo sink, *Geophys. Res. Lett.*, *31*(11), L11103, doi:10.1029/2004GL019760.

Ball, J. T. (1988), An analysis of stomatal conductance, Ph.D. thesis, Stanford Univ., Stanford, Calif.

Barry, R., T. Zhang, and D. Gilichinsky (Eds.) (2001), Russian historical soil temperature data, Natl. Snow and Ice Data Cent., Boulder, Colo. (Available at http://nsidc.org/data/arcss078.html)

Beaubien, E. G., and H. J. Freeland (2000), Spring phenology trends in Alberta, Canada: Links to ocean temperature, *Int. J. Biometeorol.*, *44*, 53–59.

Buermann, W., B. Anderson, C. J. Tucker, R. E. Dickinson, W. Lucht, C. S. Potter, and R. B. Myneni (2003), Interannual covariability in Northern Hemisphere air temperatures and greenness associated with El Niño–Southern Oscillation and the Arctic Oscillation, *J. Geophys. Res.*, *108*(D13), 4396, doi:10.1029/2002JD002630.

Cannell, M. G. R., and R. I. Smith (1983), Thermal time, chill days, and prediction of budburst in picea sitchensis, *J. Appl. Ecol.*, *20*, 951–963.

Cannell, M. G. R., and R. I. Smith (1986), Climatic warming, spring budburst, and frost damage on trees, *J. Appl. Ecol.*, *23*, 177–191.

Chapin, F. S., S. A. Zimov, G. R. Shaver, and S. E. Hobbie (1996), CO_2 fluctuation at high latitudes, *Nature*, *383*(6601), 585–586.

Chen, X. Q., and W. F. Pan (2002), Relationships among phenological growing season, time-integrated normalized difference vegetation index and climate forcing in the temperate region of eastern China, *Int. J. Climatol.*, *22*, 1781–1792.

Chuine, I. (2000), A unified model for budburst of trees, *J. Theor. Biol.*, *207*, 337–347.

Collatz, G. J., J. T. Ball, C. Grivet, and J. A. Berry (1991), Physiological and environmental regulation of stomatal conductance, photosynthesis, and transpiration: A model that includes a laminar boundary layer, *Agric. For. Meteorol.*, *54*, 107–136.

Collatz, G. J., M. Ribascarbo, and J. A. Berry (1992), Coupled photosynthesis-stomatal conductance model for leaves of C4 plants, *Aust. J. Plant Physiol.*, *19*(5), 519–538.

Conway, T. J., P. P. Tans, L. S. Waterman, K. W. Thoning, D. R. Kitzis, K. A. Masarie, and N. Zhang (1994), Evidence for interannual variability of the carbon cycle from the National Oceanic and Atmospheric Administration/Climate Monitoring and Diagnostics Laboratory Global Air Sampling Network, *J. Geophys. Res.*, *99*(D11), 22,831–22,855.

Cutforth, H. W., B. G. McConkey, R. J. Woodvine, D. G. Smith, P. G. Jefferson, and O. O. Akinremi (1999), Climate change in the semiarid prairie of southwestern Saskatchewan: Late winter–early spring, *Can. J. Plant Sci.*, *79*(3), 343–350.

Dargaville, R. J., R. M. Law, and F. Pribac (2000), Implications of interannual variability in atmospheric circulation on modeled CO_2 concentrations and source estimates, *Global Biogeochem. Cycles*, *14*(3), 931–943.

Denning, A. S., G. J. Collatz, C. Zhang, D. A. Randall, J. A. Berry, P. J. Sellers, G. D. Colello, and D. A. Dazlich (1996), Simulations of terrestrial carbon metabolism and atmospheric CO_2 in a general circulation model: Part 1. Surface carbon fluxes, *Tellus, Ser. B*, *48*, 521–542.

D'Odorico, P., J. Yoo, and S. Jaeger (2002), Changing seasons: An effect of the North Atlantic Oscillation?, *J. Clim.*, *15*, 435–445.

Farquhar, G. D., S. von Caemmerer, and J. A. Berry (1980), A biochemical model of photosynthetic CO_2 assimilation in leaves of C3 species, *Planta*, *149*, 78–90.

Hartley, S., and D. A. Robinson (2000), A shift in winter season timing in the Northern Plains of the USA as indicated by temporal analysis of heating degree days, *Int. J. Climatol.*, *20*, 365–379.

Hartmann, D. L., J. M. Wallace, V. Limpasuvan, D. W. J. Thompson, and J. R. Holton (2000), Can ozone depletion and global warming interact to produce rapid climate change?, *Proc. Natl. Acad. Sci. U. S. A.*, *97*(4), 1412–1417.

Hicke, J. A., G. P. Asner, J. T. Randerson, C. Tucker, S. Los, R. Birdsey, J. C. Jenkins, and C. Field (2002a), Trends in North American net primary productivity derived from satellite observations, 1982–1998, *Global Biogeochem. Cycles*, *16*(2), 1018, doi:10.1029/2001GB001550.

Hicke, J. A., G. P. Asner, J. T. Randerson, C. Tucker, S. Los, R. Birdsey, J. C. Jenkins, C. Field, and E. Holland (2002b), Satellite-derived increases in net primary productivity across North America, 1982–1998, *Geophys. Res. Lett.*, *29*(10), 1427, doi:10.1029/2001GL013578.

Higuchi, K., S. Murayama, and S. Taguchi (2002), Quasi-decadal variation of the atmospheric CO_2 seasonal cycle due to atmospheric circulation changes: 1979–1998, *Geophys. Res. Lett.*, *29*(8), 1173, doi:10.1029/2001GL013751.

Hoerling, M. P., J. W. Hurrell, and T. Xu (2001), Tropical origins for recent North Atlantic climate change, *Science*, *292*, 90–92.

Hunter, A. F., and M. J. Lechowicz (1992), Predicting the timing of budburst in temperate trees, *J. Appl. Ecol.*, *29*, 597–604.

Ichii, K., Y. Matsui, Y. Yamaguchi, and K. Ogawa (2001), Comparison of global net primary production trends obtained from satellite-based normalized difference vegetation index and carbon cycle model, *Global Biogeochem. Cycles*, *15*(2), 351–363.

Idso, C. D., S. B. Idso, and R. C. Balling (1999), The relationship between near-surface air temperature over land and the annual amplitude of the atmosphere's seasonal CO_2 cycle, *Environ. Exp. Bot.*, *41*(1), 31–37.

Jaagus, J., J. Truu, R. Ahas, and A. Aasa (2003), Spatial and temporal variability of climatic seasons on the East European Plain in relation to large-scale atmospheric circulation, *Clim. Res.*, *23*, 111–129.

Jackson, R. B., J. Canadell, J. R. Ehleringer, H. A. Mooney, O. E. Sala, and E. D. Schulze (1996), A global analysis of root distributions for terrestrial biomes, *Oecologia*, *108*, 389–411.

Kaduk, J., and M. Heimann (1996), A prognostic phenology scheme for global terrestrial carbon cycle models, *Clim. Res.*, *6*, 1–19.

Kalnay, E., et al. (1996), The NCEP/NCAR 40-year reanalysis project, *Bull. Am. Meteorol. Soc.*, *77*(3), 437–471.

Keeling, C. D., T. P. Whorf, M. Wahlen, and J. Vanderplicht (1995), Interannual extremes in the rate of rise of atmospheric carbon-dioxide since 1980, *Nature*, *375*(6533), 666–670.

Keeling, C. D., J. F. S. Chin, and T. P. Whorf (1996), Increased activity of northern vegetation inferred from atmospheric CO_2 measurements, *Nature*, *382*(6587), 146–149.

Keyser, A. R., J. S. Kimball, R. R. Nemani, and S. W. Running (2000), Simulating the effects of climate change on the carbon balance of North American high-latitude forests, *Global Change Biol.*, *6*, 185–195.

Kramer, K. (1994), Selecting a model to predict the onset of growth of Fagus sylvatica, *J. Appl. Ecol.*, *31*, 172–181.

Los, S. O. (1998), Linkages Between global vegetation and climate: An analysis based on NOAA Advanced Very High Resolution Radiometer data, *Rep. 1998-206852*, Goddard Space Flight Cent., Greenbelt, Md.

Los, S. O., G. J. Collatz, P. J. Sellers, C. M. Malmstrom, N. H. Pollack, R. S. DeFries, C. J. Tucker, L. Bounoua, M. T. Parris, and D. A. Dazlich (2000), A global 9-year biophysical land surface dataset from NOAA AVHRR data, *J. Hydrometeorol.*, *1*(2), 183–199.

Los, S. O., G. J. Collatz, L. Bounoua, P. J. Sellers, and C. J. Tucker (2001), Global interannual variations in sea surface temperature and land-surface vegetation, air temperature, and precipitation, *J. Clim.*, *14*, 1535–1549.

Lucht, W., I. C. Prentice, R. B. Myneni, S. Sitch, P. Friedlingstein, W. Cramer, P. Bousquet, W. Buermann, and B. Smith (2002), Climatic control of the high-latitude vegetation greening trend and Pinatubo effect, *Science*, *296*, 1687–1689.

Menzel, A. (2000), Trends in phenological phases in Europe between 1951 and 1996, *Int. J. Biometeorol.*, *44*, 76–81.

Menzel, A. (2003), Plant phenological anomalies in Germany and their relation to air temperature and NAO, *Clim. Change*, *57*(3), 243–263.

Menzel, A., and P. Fabian (1999), Growing season extended in Europe, *Nature*, *397*(6721), 659.

Murray, M. B., M. G. R. Cannell, and R. I. Smith (1989), Date of budburst of fifteen tree species in Britain following climatic warming, *J. Appl. Ecol.*, *26*, 693–700.

Myneni, R. B., C. D. Keeling, C. J. Tucker, G. Asrar, and R. R. Nemani (1997), Increased plant growth in the northern high latitudes from 1981 to 1991, *Nature*, *386*(6626), 698–702.

Nemani, , R. M. White, P. Thornton, K. Nishida, S. Reddy, J. Jenkins, and S. Running (2002), Recent trends in hydrologic balance have enhanced the terrestrial carbon sink in the United States, *Geophys. Res. Lett.*, *29*(10), 1468, doi:10.1029/2002GL014867.

Nikolov, N., and K. F. Zeller (2003), Modeling coupled interactions of carbon, water, and ozone exchange between terrestrial ecosystems and the atmosphere: I. Model description, *Environ. Pollut.*, *124*, 231–246.

Potter, C. S., S. Klooster, and V. Brooks (1999), Interannual variability in terrestrial net primary production: Exploration of trends and controls on regional to global scales, *Ecosystems*, *2*(1), 36–48.

Randerson, J. T., C. B. Field, I. Y. Fung, and P. P. Tans (1999), Increases in early season ecosystem uptake explain recent changes in the seasonal cycle of atmospheric CO_2 at high northern latitudes, *Geophys. Res. Lett.*, *26*(17), 2765–2768.

Reichenau, T. G., and G. Esser (2003), Is interannual fluctuations of atmospheric CO_2 dominated by combined effect of ENSO and volcanic aerosols, *Global Biogeochem. Cycles*, *17*(4), 1094, doi:10.1029/2002GB002025.

Russell, J. L., and J. M. Wallace (2004), Annual carbon dioxide drawdown and the Northern Annular Mode, *Global Biogeochem. Cycles*, *18*(1), GB1012, doi:10.1029/2003GB002044.

Sarmiento, J. L., and N. Gruber (2002), Sinks for anthropogenic carbon, *Phys. Today*, *55*(8), 30–36.

Schaefer, K., A. S. Denning, N. Suits, J. Kaduk, I. Baker, S. Los, and L. Prihodko (2002), Effect of climate on interannual variability of terrestrial CO_2 fluxes, *Global Biogeochem. Cycles*, *16*(4), 1102, doi:10.1029/2002GB001928.

Schaefer, K., A. S. Denning, and O. Leonard (2004), The winter Arctic Oscillation and the timing of snowmelt in Europe, *Geophys. Res. Lett.*, *31*, L22205, doi:10.1029/2004GL021035.

Scheifinger, H., A. Menzel, E. Koch, C. Peter, and R. Ahas (2002), Atmospheric mechanisms governing the spatial and temporal variability of phenological phases in central Europe, *Int. J. Climatol.*, *11*, 1739–1755.

Schwartz, M. D., and B. E. Reiter (2000), Changes in North American spring, *Int. J. Climatol.*, *20*, 929–932.

Sellers, P. J., C. J. Tucker, G. J. Collatz, S. O. Los, C. O. Justice, D. A. Dazlich, and D. A. Randall (1994), A global 1° by 1° NDVI data set for climate studies: Part II. The generation of global fields of terrestrial biophysical parameters from NDVI, *Int. J. Remote Sens.*, *15*(17), 3519–3545.

Sellers, P. J., D. A. Randall, G. J. Collatz, J. A. Berry, C. B. Field, D. A. Dazlich, C. Zhang, G. D. Collelo, and L. Bounoua (1996a), A revised land surface parameterization of GCMs: Part I. Model formulation, *J. Clim.*, *9*, 676–705.

Sellers, P. J., S. O. Los, C. J. Tucker, C. O. Justice, D. A. Dazlich, G. J. Collatz, and D. A. Randall (1996b), A revised land surface parameterization of GCMs: Part II. The generation of global fields of terrestrial biophysical parameters from satellite data, *J. Clim.*, *9*, 706–737.

Serreze, M. C., J. E. Walsh, F. S. Chapin, T. Osterkamp, M. Dyurgerov, V. Romanovsky, W. C. Oechel, J. Morison, T. Zhang, and R. G. Barry (2000), Observational evidence of recent change in the northern high-latitude environment, *Clim. Change*, *46*(1–2), 159–207.

Shabanov, N. V., L. M. Zhou, Y. Knyazikhin, R. B. Myneni, and C. J. Tucker (2002), Analysis of interannual changes in northern vegetation activity observed in AVHRR data from 1981 to 1994, *IEEE Trans. Geosci. Remote Sens.*, *40*(1), 115–130.

Shindell, D. T., R. L. Miller, G. A. Schmidt, and L. Pandolfo (1999), Simulation of recent northern winter climate trends by greenhouse-gas forcing, *Nature*, *399*(6735), 452–455.

Slayback, D. A., J. E. Pinzon, S. O. Los, and C. J. Tucker (2003), Northern Hemisphere photosynthetic trends 1982–99, *Global Change Biol.*, *9*, 1–15.

Stone, R. S., E. G. Dutton, J. M. Harris, and D. Longenecker (2002), Earlier spring snowmelt in northern Alaska as an indicator of climate change, *J. Geophys. Res.*, *107*(D10), 4089, doi:10.1029/2000JD000286.

Tanja, S., et al. (2003), Air temperature triggers the recovery of evergreen boreal forest photosynthesis in spring, *Global Change Biol.*, *9*, 1410–1426.

Thompson, D. W. J., and J. M. Wallace (2000), Annular modes in the extratropical circulation: Part I. Month-to-month variability, *J. Clim.*, *13*, 1000–1016.

Thompson, D. W. J., and J. M. Wallace (2001), Regional climate impacts of the Northern Hemisphere annular mode, *Science*, *293*, 85–89.

Thompson, D. W. J., J. M. Wallace, and G. Hegerl (2000), Annular modes in the extratropical circulation: Part II. Trends, *J. Clim.*, *13*, 1018–1036.

Tucker, C. J., D. A. Slayback, J. E. Pinzon, S. O. Los, R. B. Myneni, and M. G. Taylor (2001), Higher northern latitude normalized difference vegetation index and growing season trends from 1982 to 1999, *Int. J. Biometeorol.*, *45*, 184–190.

Vaganov, E. A., M. K. Hughes, A. V. Kirdyanov, F. H. Schweingruber, and P. P. Silkin (1999), Influence of snowfall and melt timing on tree growth in subarctic Eurasia, *Nature*, *400*(6740), 149–151.

White, M. A., P. E. Thornton, and S. W. Running (1997), A continental phenology model for monitoring vegetation responses to interannual climatic variability, *Global Biogeochem. Cycles*, *11*(2), 217–234.

White, M. A., S. W. Running, and P. E. Thornton (1999), The impact of growing season length variability on carbon assimilation and evapotranspiration over 88 years in the eastern US deciduous forest, *Int. J. Biometeorol.*, *42*, 139–145.

Wu, W. L., and A. H. Lynch (2000), Response of the seasonal carbon cycle in high latitudes to climate anomalies, *J. Geophys. Res.*, *105*(D18), 22,897–22,908.

Zhang, C., D. A. Dazlich, D. A. Randall, P. J. Sellers, and A. S. Denning (1996), Calculation of the global land surface energy, water, and CO_2 fluxes with an off-line version of SiB2, *J. Geophys. Res.*, *101*(D14), 19,061–19,075.

Zhou, L. M., C. J. Tucker, R. K. Kaufmann, D. Slayback, N. V. Shabanov, and R. B. Myneni (2001), Variations in northern vegetation activity inferred from satellite data of vegetation index during 1981 to 1999, *J. Geophys. Res.*, *106*(D17), 20,069–20,083.

Zhou, L., R. K. Kaufmann, Y. Tian, R. B. Myneni, and C. J. Tucker (2003), Relation between interannual variations in satellite measures of northern

forest greenness and climate between 1982 and 1999, *J. Geophys. Res.*, *108*(D1), 4004, doi:10.1029/2002JD002510.

Zimov, S. A., S. P. Davidov, Y. V. Voropaev, S. F. Prosiannikov, I. P. Semiletov, M. G. Chapin, and F. S. Chapin (1996), Siberian CO_2 efflux in winter as a CO_2 source and cause of seasonality in atmospheric CO_2, *Clim. Change*, *33*(1), 111–120.

Zimov, S. A., S. P. Davidov, G. M. Zimova, A. I. Davidova, F. S. Chapin, M. C. Chapin, and J. F. Reynolds (1999), Contribution of disturbance to increasing seasonal amplitude of atmospheric CO_2, *Science*, *284*, 1973–1976.

A. S. Denning, O. Leonard, and K. Schaefer, Department of Atmospheric Science, Colorado State University, Fort Collins, CO 80523, USA. (kevin@atmos.colostate.edu)